

## RESEARCH OUTPUTS / RÉSULTATS DE RECHERCHE

### COMPLEX CONTAGION IN SOCIAL SYSTEMS WITH DISTRUST

de Kemmeter, Jean-François; Gallo, Luca; Boncoraglio, Fabrizio; Latora, Vito; Carletti, Timoteo

*Published in:*  
Advances in Complex Systems

*DOI:*  
[10.1142/S0219525924400010](https://doi.org/10.1142/S0219525924400010)

*Publication date:*  
2024

*Document Version*  
Publisher's PDF, also known as Version of record

#### [Link to publication](#)

*Citation for published version (HARVARD):*

de Kemmeter, J-F, Gallo, L, Boncoraglio, F, Latora, V & Carletti, T 2024, 'COMPLEX CONTAGION IN SOCIAL SYSTEMS WITH DISTRUST', *Advances in Complex Systems*, vol. 27, no. 4-5, 2440001.  
<https://doi.org/10.1142/S0219525924400010>

#### General rights

Copyright and moral rights for the publications made accessible in the public portal are retained by the authors and/or other copyright owners and it is a condition of accessing publications that users recognise and abide by the legal requirements associated with these rights.

- Users may download and print one copy of any publication from the public portal for the purpose of private study or research.
- You may not further distribute the material or use it for any profit-making activity or commercial gain
- You may freely distribute the URL identifying the publication in the public portal ?

#### Take down policy

If you believe that this document breaches copyright please contact us providing details, and we will remove access to the work immediately and investigate your claim.

# Complex contagion in social systems with distrust

Jean-François de Kemmeter,<sup>1,2,\*</sup> Luca Gallo,<sup>3</sup> Fabrizio Boncoraglio,<sup>4,5</sup> Vito Latora,<sup>6,7,8,9</sup> and Timoteo Carletti<sup>1,†</sup>

<sup>1</sup>*Department of Mathematics and naXys, Namur Institute for Complex Systems,  
University of Namur, Rue Grafé 2, B5000 Namur, Belgium*

<sup>2</sup>*Department of Mathematics, Florida State University,  
1017 Academic Way, Tallahassee, FL 32306, United States of America*

<sup>3</sup>*Department of Network and Data Science, Central European University, Quellenstraße 51, 1100 Vienna, Austria*

<sup>4</sup>*Department of Applied Science and Technology, Politecnico of Turin,  
Corso Duca degli Abruzzi 24, 10129 Turin, Italy*

<sup>5</sup>*Scuola Superiore di Catania, Via Valdisavoia 9, 95123 Catania, Italy*

<sup>6</sup>*School of Mathematical Sciences, Queen Mary University of London, London E1 4NS, UK*

<sup>7</sup>*Department of Physics and Astronomy, University of Catania, 95125 Catania, Italy*

<sup>8</sup>*INFN Sezione di Catania, Via S. Sofia, 64, 95125 Catania, Italy*

<sup>9</sup>*Complexity Science Hub Vienna, A-1080 Vienna, Austria*

Social systems are characterized by the presence of group interactions and by the existence of both trust and distrust relations. Although there is a wide literature on signed social networks, where positive signs associated to the links indicate trust, friendship, agreement, while negative signs represent distrust, antagonism, and disagreement, very little is known about the effect that signed interactions can have on the spreading of social behaviours when, not only pairwise, but also higher-order interactions are taken into account. In this paper we introduce a model of complex contagion on signed simplicial complexes, and we investigate the role played by trust and distrust on the dynamics of a social contagion process, where exposure to multiple sources is needed for the contagion to occur. The presence of higher-order signed structures in our model naturally induces new infection and recovery mechanisms, thus increasing the richness of the contagion dynamics. Through numerical simulations and analytical results in the mean-field approximation, we show how distrust determines the way the system moves from a state where no individuals adopt the social behavior, to a state where a finite fraction of the population actively spreads it. Interestingly, we observe that the fraction of spreading individuals displays a non-monotonic dependence with respect to the average number of connections between individuals. We then investigate how social balance affects social contagion, finding that balanced triads have an ambivalent impact on the spreading process, either promoting or impeding contagion based on the relative abundance of fully trusted relations. Our results shed light on the nontrivial effect of trust on the spreading of social behaviors in systems with group interactions, paving the way to further investigations of spreading phenomena in structured populations.

## I. INTRODUCTION

Contagion is the process through which a disease, an opinion, a behavior or a technological innovation spreads in a population of interacting individuals [1]. While some spreading processes only require a single exposure for a contagion to occur, others are only triggered by multiple exposures. In the first case, the spreading process is referred to as *simple contagion*, while in the latter case it is known as *complex contagion* [2]. The spread of an infectious disease in a population is a typical example of a simple contagion [3], while the propagation of a social behavior, such as the adoption of a social norm, of an opinion, or even a novel item can be characterized either as a simple [4] or a complex contagion [5]. In particular in social contagion there are cases where the individuals/agents of a social system can either accept or refuse transmission, based on the type of their social interactions, instead of just passively receive it as in the case of

a virus [6, 7].

The spread of a social behavior in a population is utterly determined by the precise patterns of interactions among individuals. Usually, the structure of contacts in a social system is mathematically modeled as a graph, whose nodes represent the individuals, the social agents, while the edges encode for their pairwise interactions [8]. Without surprise thus, the contagion process is shaped by the structure of such graph, for instance by its modular organization, the existence of short paths, weak ties or influential nodes [9–12]. Complex contagion on networks has been notably analyzed using threshold models, where a susceptible individual becomes infected if a sufficiently large fraction of its neighbors is infected [13, 14].

Although network science provides powerful tools to model dynamical processes in social systems, the network approach has strong limitations in dealing with group interactions. The latter are indeed a fundamental ingredient of social systems and result to be a main driver for social contagion [15]. As a consequence, last years have seen a growing interest in higher-order networks, namely mathematical structures generalizing complex networks and accounting for group interactions [16–20]. Recent

---

\* jean-francois.dekemmeter@unamur.be

† timoteo.carletti@unamur.be

works on social contagion on higher-order networks have demonstrated that peer pressure and group reinforcement can induce novel phenomena, such as the appearance of abrupt phase transitions and bistability [15, 21–26]. One aspect that still has not been considered and explored exhaustively is the role that trust/distrust can have on the diffusion of a novel idea or item, or in the adoption of a social norm. Trust among individuals is a key driver of contagion in social systems: agents are more prone to adopt a novel behavior if it comes from trusted sources, a behaviour recalling the “repelling rule” [7]. Moreover, infected agents, i.e., agents having adopted a given item, when they interact with other infected agents that they do not trust, can decide to stop adopting the item. The rationale behind the latter process is that two agents that distrust each other would not be inclined to share the same item. Some researches have already started to investigate the impact of trust on social contagion and epidemic spreading on networks [27–29], but no work has yet considered contagion processes on signed higher-order networks.

In this paper we propose a model of complex contagion on signed higher-order networks, which allows to investigate the impact of trust and distrust among individuals on the spread of contagion in a social system, by properly taking into account interactions in groups of two or more individuals at the microscopic level. Our model is inspired by the model of complex contagion on simplicial complexes proposed in Ref. [15]. Indeed, as the underlying structure of the social system we consider a simplicial complex instead of a network. A simplicial complex is a made not only by nodes and by links connecting pairs of nodes, and representing pairwise interactions between individuals, but also by more complex objects, which represent interactions in groups of more than two individuals. We then extend the model of Ref. [15] by introducing positive and negative signs over the links of the simplicial complex, allowing us to study the role of trust on complex simplicial social contagion. It is however a common experience that the trust/distrust relations existing between two individuals can change once the two individuals are interacting into a group of larger size. For this reason we propose and analyze two variants of our social contagion model. In the first version of the model we assume that the signs of the pairwise interactions remain the same also in higher-order interactions. In the second one, we relax such an assumption allowing agents to exhibit pairwise trust/distrust relations different from those experienced in groups involving more than two individuals. Namely, in order to determine the distribution of signed relations in a group interactions, we recur to *social balance* theory [30–35]. According to this theory a group of three individuals, a triad, is balanced when there is an odd number of positive relations among them [36]. Thus we have two distinct balanced configurations that can be interpreted either as “the friend of my friend is my friend” in case of three trust relations, or “the enemy of my enemy is my friend” in presence of a single trust rela-

tion. Both of these configurations ensure the consistency of the members’ attitude with respect to each other. At contrast, a triad in which there is an even number of trust relations leads unavoidably to some kind of frustration among the individuals in the triad as it implies that the “friend of my friend is my enemy” or that “the enemy of my enemy is my enemy”, both cases being unwanted by its members. For this reason we expect these types of triads to appear less frequently. Therefore, in the second version of the model we introduce new parameters to tune the distribution of different configurations in the signed simplicial complexes. This allows us to investigate the impact of balanced and unbalanced triangles on social contagion.

With the first model, we show how the level of distrust in the social network determines the nature of the transition, i.e., continuous or discontinuous, from a state where no individual adopts the social behavior, i.e., disease-free state, to a regime where a fraction of agents spread it, i.e., to an endemic state. Particularly, we show that the size of the endemic state can be a non-monotonic function of the average node degree, depending of the level of distrust in the population. With the second model, we analyze the ambivalent role of social balance, showing that simplicial complexes where balanced triads are overrepresented compared to the random case can either promote or impede contagion. In particular, we find that the abundance of triangles with three positive signs enhances the emergence of a bistable regime and thus lets the system easily switch to an endemic state. We also show that the other balanced configuration, i.e., two negative signs, induces instead the opposite behavior. Similar results are also presented when investigating the role of unbalanced triangles.

We corroborate our analytical findings by comparing the mean-field predictions to stochastic simulations performed by using a Gillespie algorithm [37].

The paper is organized as follows. In Section II, we introduce our model of complex contagion on signed simplicial complexes. In Section III, we derive the mean-field equations of the model, while in Section IV, we determine the equilibrium solutions of the system and examine their stability, assuming a random distribution of edge signs, namely under the assumption of the first model. In section V, we introduce the second version of the model, and we investigate how structural balance affects contagion. We then conclude with some future perspectives.

## II. MODELING SOCIAL CONTAGION WITH TRUST AND DISTRUST

In the context of pairwise interactions, trust and distrust relations between individuals are represented as links associated with signs, respectively positive or negative. Inspired by this observation, to model group interactions with trust or distrust we will use signed simplices. A  $q$ -simplex,  $\sigma$ , is a set of  $q+1$  nodes such that any subset

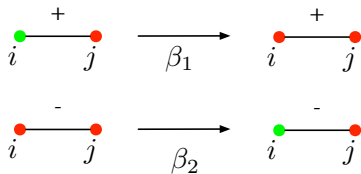


FIG. 1. **Infection and recovery in signed pairwise interactions.** A susceptible agent (green) gets infected (red) by a trusted infected agent (top panel) with a rate  $\beta_1 > 0$ . An infected agent recovers, when in contact with a distrusted infected agent (bottom panel), with a rate  $\beta_2 > 0$ . In all the remaining pairwise configurations the agent will not change its state.

of the nodes also belongs to the  $q$ -simplex. Such subsets are referred to as the faces of the simplex. In particular, 0-simplices are the nodes, 1-simplices correspond to edges and denote pairwise interactions, 2-simplices are triangles and encode three-body interactions, and so on so forth [38]. To model trust and distrust, each node in a  $q$ -simplex,  $q \geq 1$ , is endowed with a positive or negative sign toward each of the remaining  $q$  nodes of the simplex. For simplicity, we assume (dis)trust relations to be reciprocal. Let us observe that in real social systems the existence of a (dis)trust relation between two individuals in a pairwise interaction does not imply that the same (dis)trust relation exists when a third person is involved in the interaction.

In our model, individuals are assumed to be either in an infected state, i.e., they are spreading a given social behavior, or in a susceptible state, i.e., they are not. Note that we will hereafter keep using the vocabulary of epidemic processes. In particular, we will consider infections, i.e., mechanisms for which an individual starts spreading a social behavior after interacting with other individuals, and recoveries, i.e., mechanisms for which an individual stops spreading the behavior. Differently from epidemic spreading, in our model we assume that an individual can stop spreading the social behavior both independently or after having interacted with other individuals. This recovery process mediated by other individuals does not have a counterpart in epidemic spreading, where the recovery from a disease occurs spontaneously. Furthermore, we will denote endemic state the condition of the system where a positive fraction of individuals are infected, i.e., they adopt and spread the social behavior, and we will refer to the threshold above which an endemic state emerges as epidemic threshold.

In our model, we assume that infection and recovery processes can take place at three distinct levels, namely at the level of single individuals, i.e., 0-simplices, at the level of pairwise contacts, i.e., 1-simplices, and also at the level of three-body interactions, 2-simplices. To present our results in a simple and direct way, we limit our analysis here to simplices up to order  $q = 2$ . This assumption is motivated by the fact that larger interacting groups are less abundant compared to smaller groups [39]. In addition,

although our modeling approach can be extended to larger group sizes [21], considering larger group size interactions would make the analysis more involved. At the level of 0-simplices, we only have recovery processes, with infected individuals coming back to the susceptible state with a rate  $\mu$ , namely they stop spreading after an average time  $1/\mu$ . At the level of 1-simplices, two processes are at play, an infection process and a recovery one. For the infection process, a susceptible individual gets infected with a rate  $\beta_1 > 0$  when interacting with a trusted infected individual (see top panel of Fig. 1). For the recovery process, if an infected individual interacting with a distrusted infected individual becomes susceptible with a rate  $\beta_2 > 0$  (see bottom panel of Fig. 1). Nonlinear recovery processes in social contagion have not been extensively adopted, with a few exceptions [40], and in our case the rationale is that individuals that do not trust each other are less willing to adopt and spread the same social behavior. Beyond contagion processes, it is worth mentioning that negative dynamics has been considered in the consensus problem [7, 41]. In particular, the *repelling negative dynamics* on signed networks, where agents are attracted to each other if a positive link connects them, while they repel each other if there is a negative link between them, has been analyzed in the last years [7]. For such a process, the system may not converge to a consensus state due to the presence of negative links [7]. Similarly, as we will show in the following, negative connections can affect the contagion dynamics, limiting the spread of the social behavior in the system.

In the case of three-body interactions, we consider five different processes, namely three types of infections and two types of recoveries. An individual can change state by interacting with two infected individuals, with a rate that depends on the trust/distrust relations existing among the three agents. This comes from the assumption that, when interacting in group, each agent has full knowledge of all the trust/distrust relations existing among the group members. Note that this is a reasonable assumption in the case of small groups. Let us first consider the cases in which a susceptible individual,  $i$ , participates in a three-body interaction with two infected ones,  $j$  and  $k$  (see Fig. 2).

**Case 1:** If all the agents trust each other, i.e., there are three “+” signs in the 2-simplex, then the susceptible individual  $i$  becomes infected with a rate  $\gamma_1 > 0$ .

**Case 2:** If  $i$  trusts  $j$  and  $k$  but there is a distrust relation between  $j$  and  $k$ ,  $i$  can still be infected, but with a positive rate  $\gamma_2 \leq \gamma_1$ . This comes from the idea that the distrust relation existing among  $j$  and  $k$  can negatively influence the propensity of  $i$  to adopt the social behavior.

**Case 3:** If a susceptible agent  $i$  trusts agent  $j$  but distrusts agent  $k$ , while there is a trust relation between  $j$  and  $k$ , then  $i$  becomes infected with a positive rate  $\gamma_3 \leq \gamma_2$ . As in the previous case, the presence of a distrust relation determines a decrease in the adoption rate of agent  $i$ , even more than in the case of the second mechanism, as agent  $i$  directly experience distrust.

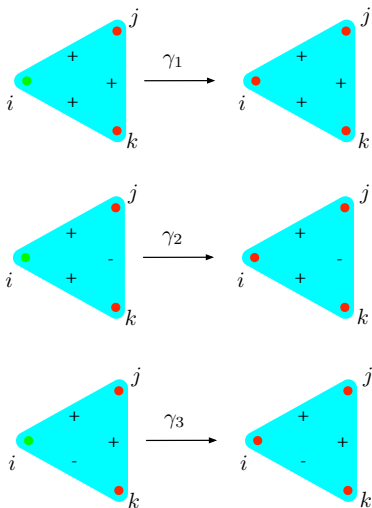


FIG. 2. **Infection in groups of size 3 with signed relations.** A susceptible agent (green) becomes infected (red) because of an interaction in a group of size 3 (cyan triangle). In the top panel the agents experience three trust relations, in the middle panel there is distrust between the two infected nodes  $j$  and  $k$ , and in the bottom panel there is distrust between  $i$  and  $k$ , i.e., a susceptible and an infected node. In all three cases the susceptible agent will get infected but with rates  $\gamma_1 \geq \gamma_2 \geq \gamma_3 \geq 0$ .

We now consider the cases where three infected individuals, experiencing distrust relations, interact (see Fig. 3).

**Case 4:** If an agent  $i$  distrusts both  $j$  and  $k$ , perceiving a trust relation between them, it will become susceptible with a rate  $\gamma_4 \geq 0$ .

**Case 5:** If the three agents distrust each other, one of them can still become susceptible, but at a smaller rate, i.e.,  $0 \leq \gamma_5 \leq \gamma_4$ . In both cases, the rationale is that distrust can induce doubt, pushing the agents to stop adopting the social behavior. It is worth remarking that our model involves a larger variety of infection and recovery mechanisms compared to the model proposed in Ref. [15]. In particular, in the simplicial contagion model [15] only positive interactions are considered. Therefore, the model is governed only by two infection processes, namely the two-body and one of the three-body contagions (i.e., Case 1). Instead, considering negative links leads to additional three-body infection processes, as well as a set non-linear recovery mechanisms, which do not find correspondence in the simplicial contagion model.

So far, we have described the microscopic mechanisms, occurring at the level of  $q$ -simplices, underlying our model of social contagion with trust and distrust. However, the macroscopic spreading of social behaviors within a population is determined by the precise patterns of interaction among individuals. To model the complex structure of interactions in a real social systems, we rely on signed simplicial complexes. Given a

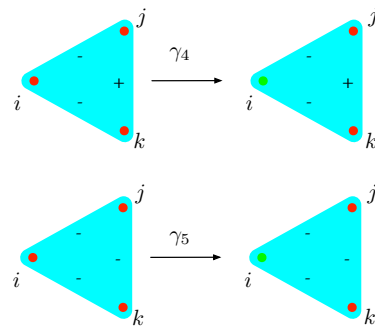


FIG. 3. **Recovery in groups of size 3 with signed relations.** An infected agent (red) becomes susceptible (green) because of the interaction in a group of size 3 (cyan triangle). In the top panel agent  $i$  experiences a distrust relation with  $j$  and  $k$ , and at the same time perceives a trust relation between  $j$  and  $k$ . In the bottom panel all the agents distrust each other. In both cases  $i$  will become susceptible, in the former case with a rate  $\gamma_4 \geq 0$ , in the latter with a rate  $\gamma_5 \geq 0$ , such that  $\gamma_4 \geq \gamma_5 \geq 0$ .

set  $\mathcal{V} = \{1, \dots, N\}$  of nodes, a simplicial complex  $\mathcal{K}$  is a collection of signed simplices, with an inclusion requirement, meaning that for any simplex  $\sigma \in \mathcal{K}$ , all simplices  $\tau \subset \sigma$  are also contained in  $\mathcal{K}$ . Let us observe that the inclusion property means, for example, that if three people interact altogether, then each of them will also interact pairwise with the two others. In the following, we will denote by  $\eta \in [0, 1]$  the fraction of 1-simplices (the links) with a minus sign in the simplicial complex, i.e., the fraction of dyadic relations based on distrust. Let us observe that besides the epidemic parameters and the number of trust/distrust relations, our model of social contagion will also depend on the topological features of the simplicial complex representing the interactions among the individuals, e.g., the arrangement of trust/distrust relations, the average number of 1 and 2-simplices incident to a node, and so on. In the following we will focus on the impact of the distrust using mean-field equations and stochastic simulations.

### III. MEAN-FIELD EQUATIONS

Let us now cast the microscopic mechanisms discussed so far into an ODE model for the fraction  $\rho(t)$  of infected agents at time  $t$ . Working in a mean-field approximation that neglects 2-nodes correlations, we get:

$$\begin{aligned} \frac{d\rho}{dt} = & -\mu\rho + \beta_1\rho(1-\rho)\ell_1 - \beta_2\rho^2\ell_0 \\ & + \gamma_1\rho^2(1-\rho)\tau_3 + \frac{\gamma_2}{3}\rho^2(1-\rho)\tau_2 + \frac{2\gamma_3}{3}\rho^2(1-\rho)\tau_2 \\ & - \frac{\gamma_4}{3}\rho^3\tau_1 - \gamma_5\rho^3\tau_0, \end{aligned} \quad (1)$$

where  $\ell_1$  (resp.  $\ell_0$ ) is the mean number of trust links, i.e., links with a “+” sign (resp. distrust links, i.e., with a “-” sign), which are incident in a node. We can write

$\ell_1 = (1 - \eta)\langle k \rangle$ , and thus  $\ell_0 = \eta\langle k \rangle$ , where  $\langle k \rangle$  is the average node degree, i.e. the average number of edges incident to a node, and  $\eta$  the fraction of negative links existing in the social network. For  $m \in \{0, 1, 2, 3\}$ , the mean number of triangles with  $m$  trust relations, i.e.,  $m$  “+” signs, is denoted by  $\tau_m$ .

The different terms in the first line of Eq. (1) respectively model (from the left to right) the standard (single-node) recovery, the infection due to a pairwise interaction between a susceptible and an infected person trusting each other, and finally the recovery of an infected agent because of a dyadic interaction involving two distrusting infected agents (i.e., the processes described in Fig. 1). The second line, again from left to right, describes a contagion due to a triadic interaction involving two infected and one susceptible agent, all trusting each other (see top panel of Fig. 2). A contagion occurring in a triadic group with two infected and one susceptible people, the latter trusting the two others who do not trust each other; the factor  $1/3$  represents the fact that, focusing on one node, only one third of all triangles with two “+” and one “-” has the right configuration of signs (see middle panel of Fig. 2). Finally, a contagion due to again a triadic interaction with two infected individuals and a susceptible one, where the susceptible person trusts one person but not the other one. The factor  $2/3$  again is due to the fact that only a fraction  $2/3$  of such triangles has the right signs setting (see bottom panel of Fig. 2). The third line of Eq. (1) denotes the recovery of an infected person because of a triadic interaction involving three infected people, the former one distrusting the latter two, from which the factor  $1/3$  follows. Then a recovery process involving three mutually distrusting infected people (see Fig. 3).

Gathering together powers of  $\rho$  we can rewrite Eq. (1) as follows:

$$\frac{d\rho}{dt} = \rho (a + b\rho + c\rho^2), \quad (2)$$

where

$$\begin{aligned} a &= -\mu + \beta_1(1 - \eta)\langle k \rangle \\ b &= -\beta_1(1 - \eta)\langle k \rangle - \beta_2\eta\langle k \rangle + \gamma_1\tau_3 + \frac{\gamma_2\tau_2}{3} + \frac{2\gamma_3\tau_2}{3} \\ c &= -\gamma_1\tau_3 - \frac{\gamma_2\tau_2}{3} - \frac{2\gamma_3\tau_2}{3} - \frac{\gamma_4}{3}\tau_1 - \gamma_5\tau_0. \end{aligned}$$

#### IV. STATIONARY DENSITIES: EXISTENCE AND STABILITY

We are now interested in finding the stationary solutions of Eq. (1) and in studying their stability. This will allow us to investigate the asymptotic behavior of our system and to draw conclusion on the conditions leading to the emergence on an endemic state. Let us start by assuming that the three agents taking part in a three-body interaction maintain the same trust and distrust

relations they have in pairwise interactions, meaning that the signs of the three-body interaction are directly “inherited” from the three underlying pairs. This will allow us to draw some preliminary conclusions on the role of trust on contagion. We will then relax such an hypothesis and present a more general setting in the following section. Under this working assumption, we can write

$$\begin{aligned} \tau_0 &= \eta^3\langle k_\Delta \rangle, \tau_1 = 3\eta^2(1 - \eta)\langle k_\Delta \rangle \\ \tau_2 &= 3\eta(1 - \eta)^2\langle k_\Delta \rangle \text{ and } \tau_3 = (1 - \eta)^3\langle k_\Delta \rangle, \end{aligned}$$

where  $\langle k_\Delta \rangle$  is the average number of 2-simplices incident to a node. We can thus determine the stationary solutions of the mean-field equations and their stability. Beside the disease free equilibrium  $\rho_0^* = 0$ , that is always a solution, there can be other two solutions given by:

$$\rho_\pm^* = \frac{\Lambda - \tilde{\lambda}_1 - \lambda_2 \pm \sqrt{(\Lambda - \tilde{\lambda}_1 - \lambda_2)^2 - 4(\Lambda + \tilde{\Lambda})(1 - \tilde{\lambda}_1)}}{2(\Lambda + \tilde{\Lambda})}, \quad (3)$$

if  $(\Lambda - \tilde{\lambda}_1 - \lambda_2)^2 - 4(\Lambda + \tilde{\Lambda})(1 - \tilde{\lambda}_1) > 0$  and the parameters are such that  $\rho_\pm^* \in (0, 1)$ , where  $\Lambda := \Lambda_1 + \Lambda_2 + \Lambda_3$  and  $\tilde{\Lambda} := \Lambda_4 + \Lambda_5$  with:

$$\Lambda_1 = \frac{\gamma_1\tau_3}{\mu}, \Lambda_2 = \frac{\gamma_2\tau_2}{3\mu}, \Lambda_3 = \frac{2\gamma_3\tau_2}{3\mu}, \quad (4)$$

$$\Lambda_4 = \frac{\gamma_4\tau_1}{3\mu} \text{ and } \Lambda_5 = \frac{\gamma_5\tau_0}{\mu}, \quad (5)$$

$$\tilde{\lambda}_1 := \lambda_1(1 - \eta) = \frac{\beta_1\langle k \rangle}{\mu}(1 - \eta), \lambda_2 = \frac{\beta_2\eta\langle k \rangle}{\mu}. \quad (6)$$

We notice that, in the special case where all agents trust each other, i.e., when  $\eta = 0$ , we have  $\tilde{\Lambda} = 0, \lambda_2 = 0, \Lambda = \lambda_\Delta := \frac{\gamma_1 k_\Delta}{\mu}$  and  $\tilde{\lambda}_1 = \lambda_1 := \frac{\beta_1\langle k \rangle}{\mu}$  and we recover the fixed points obtained in [15]. In this case, it has been shown that the epidemic threshold is given by  $\lambda_1 = 1$  and that the transition at the epidemic threshold is continuous when  $\lambda_\Delta \leq 1$  and discontinuous otherwise; in that case the system shows bistability for an interval of values of  $\lambda_1$ , i.e., it admits as stable equilibria both the disease free state and the endemic state. In the following we show how the analysis can be extended to the general case where  $0 < \eta \leq 1$ .

By rescaling time by  $\mu$  and linearizing (2) close to the equilibrium  $\rho_0^* = 0$ , we can realize that the latter is stable if and only if  $\tilde{\lambda}_1 = \lambda_1(1 - \eta) < 1$ . Hence, we find that the epidemic threshold for the disease free equilibrium is given by  $\lambda_1 = 1/(1 - \eta)$ . Above this threshold, the infection will always spread and reach a non-zero fraction of the population, while below this threshold the infection will die out unless the fraction of initially infected nodes is sufficiently large, i.e., above a critical mass. In that case nonlinear terms might sustain the disease. Crucially, we observe that the epidemic threshold increases as  $\eta$  becomes larger (see top panel of Fig. 4). This means that distrust can limit the spreading of the infection, as a large value of  $\lambda_1$  is needed to initiate the contagion process. Let us now analyze the existence and the stability

of the aforementioned fixed points  $\rho_{\pm}^*$ , as a function of  $\tilde{\lambda}_1$ . We refer to Appendix A for a detailed derivation of the stability of the fixed points.

- By looking at the definition of  $\rho_{\pm}^*$  one can realize that if  $0 < \tilde{\lambda}_1 < \lambda_{crit}$  then  $\rho_{\pm}^*$  assume complex values, where  $\lambda_{crit} = -(\lambda_2 + \Lambda + 2\tilde{\Lambda}) + 2\sqrt{(\Lambda + \tilde{\Lambda})(1 + \lambda_2 + \tilde{\Lambda})} < 1$  as one can observe by rewriting it as follows

$$\begin{aligned} \lambda_{crit} &= -(\lambda_2 + 1 + \tilde{\Lambda}) - (\Lambda + \tilde{\Lambda}) + 1 \\ &\quad + 2\sqrt{(\Lambda + \tilde{\Lambda})(1 + \lambda_2 + \tilde{\Lambda})} \\ &= -\left[\sqrt{\lambda_2 + \Lambda + \tilde{\Lambda}} - \sqrt{\Lambda + \tilde{\Lambda}}\right]^2 + 1 < 1. \end{aligned}$$

- If  $\lambda_{crit} < \tilde{\lambda}_1 < 1$  and  $1 + \lambda_2 > \Lambda$ , then  $\rho_{\pm}^*$  are real but negative, so they are not physically acceptable.
- If  $\lambda_{crit} < \tilde{\lambda}_1 < 1$  and  $1 + \lambda_2 < \Lambda$ , then  $\rho_{\pm}^*$  are real and positive, so they are both physically acceptable, moreover  $\rho_-^*$  is unstable while  $\rho_+^*$  is stable.
- If  $\tilde{\lambda}_1 > 1$ ,  $\rho_{\pm}^*$  are real but  $\rho_-^*$  is negative, thus the only physically acceptable solution is  $\rho_+^*$  which is stable.

By considering the behavior of the solutions  $\rho_{\pm}^*$  for large  $\tilde{\lambda}_1$ , we can prove that  $\rho_+^* \rightarrow 1$ . In Table I we summarize the different asymptotic solutions of Eq. (2) and their stability as a function of the involved parameters.

The above analysis allows us to conclude that when  $\Lambda > 1 + \lambda_2$ , the prevalence of infected individuals has a discontinuous phase transition at  $\tilde{\lambda}_1 = \lambda_{crit}$  and it is bistable for  $\lambda_{crit} < \tilde{\lambda}_1 < 1$ . On the other hand when  $\Lambda < 1 + \lambda_2$ , the transition from the disease-free state to the endemic state is instead continuous.

The different dynamical regimes of the model, listed in Table I, can be understood as follows. In an infinitesimal time interval  $[t, t + dt]$ , the probability that a node will spontaneously recover is given by  $\mu dt$  while the probability that it will get infected due to a pairwise infection is given by  $\beta_1 \langle k \rangle (1 - \eta) dt$ . If the ratio  $\lambda_1 := \beta_1 \langle k \rangle (1 - \eta) / \mu$  is larger than 1, then the pairwise infection is strong enough compared to the spontaneous recovery and the epidemic will always propagate. On the contrary, when  $\lambda_1 < 1$ , the infection is predicted to become extinct in the absence of higher-order group interactions but can persist if  $\Lambda > 1 + \lambda_2$ . The latter condition has the following interpretation:  $\mu \Lambda dt$  is the probability that a susceptible node will get infected due to a three-body infection while  $\mu(1 + \lambda_2) dt$  is the probability that an infected node will recover either spontaneously or due to a pairwise interaction. Hence, if the rates associated with the three-body infection channels are large enough, they might sustain the epidemic even below the epidemic threshold. It is worth noting an important difference between this result

and the one found for the simplicial contagion model [15]. Both  $\Lambda$  and  $\lambda_2$  depend on the fraction of negative links  $\eta$ : the former decreases as  $\eta$  gets larger, while the latter is positively correlated with  $\eta$ . Therefore, the level of distrust in the system can impact the ability of higher-order interactions to sustain the contagion process. Also, in our model, higher-order infections oppose the effect of both linear and non-linear recoveries, while in the simplicial contagion model, only linear recoveries exist. This effect is recovered by setting  $\eta = 0$ , i.e., only positive links are present, as the inequality  $\Lambda > 1 + \lambda_2$  becomes  $\Lambda_1 > 1$ , which is the relation obtained in Ref. [15].

TABLE I. Number and stability of stationary density of infected people depending on the parameters  $\tilde{\lambda}_1$  and  $\Lambda$ .

$\tilde{\lambda}_1 < \lambda_{crit}$	$\lambda_{crit} < \tilde{\lambda}_1 < 1$ $\Lambda < 1 + \lambda_2$	$\lambda_{crit} < \tilde{\lambda}_1 < 1$ $\Lambda > 1 + \lambda_2$	$\tilde{\lambda}_1 \geq 1$
$\rho_0^* = 0$ (stable)	$\rho_0^* = 0$ (stable)	$\rho_0^* = 0$ and $\rho_+^*$ (stable)	$\rho_+^*$ (stable)
		$\rho_-^*$ (unstable)	$\rho_0^*$ (unstable)

### A. Impact of $\eta$ on bistability

Results reported in Fig. 4 show that the prevalence  $\rho^*$  increases with  $\lambda_1 = \frac{\beta_1 \langle k \rangle}{\mu}$  and as previously stated  $\rho^* \rightarrow 1$  for unbounded values of  $\lambda_1$ . To simplify the analysis, we make a few assumptions on the model parameters. First, we set  $\gamma_3 = 0$  with  $\gamma_2 \neq 0$ , as they have a similar effect on the model, i.e., changing the value of  $\Lambda$ , thus the nature of the phase transition. Second, we set  $\gamma_5 = 0$ , as the parameter  $\tilde{\Lambda}$ , which depends on  $\gamma_5$ , does not affect the phase transitions of the model. We set, however,  $\gamma_4 \neq 0$ , so to keep at least one of the higher-order recovery mechanism of the system. The mean-field predictions (curves) are compared with stochastic simulations (points) obtained by using the Gillespie algorithm. Stochastic simulations were performed on top of synthetic simplicial complexes, built by using a procedure identical to the one described in [15]. From Fig. 4 we can appreciate the good agreement between the mean-field findings and the numerical ones, confirming thus the validity of the used assumptions.

Let us now briefly review the way the simplicial complexes have been built, and refer the interested reader to Appendix B for a more detailed description of this procedure as well as the Gillespie algorithm. The construction of synthetic simplicial complexes is similar to the one used for generating Erdős-Rényi graphs. Specifically, being the number of nodes fixed in advance, we run over every pair of nodes and connect them with a probability  $p_1$ . Similarly, we run over every triplet of nodes, adding a 2-simplex among them with a probability  $p_2$ . The probabilities  $p_1$  and  $p_2$  are chosen in advance so that each node has, on average,  $\langle k \rangle$  edges and  $\langle k_{\Delta} \rangle$  triangles incident to it. The relation between the average degrees  $\langle k \rangle$ ,  $\langle k_{\Delta} \rangle$ , and the probabilities  $p_1$ ,  $p_2$  is recalled in Appendix B.

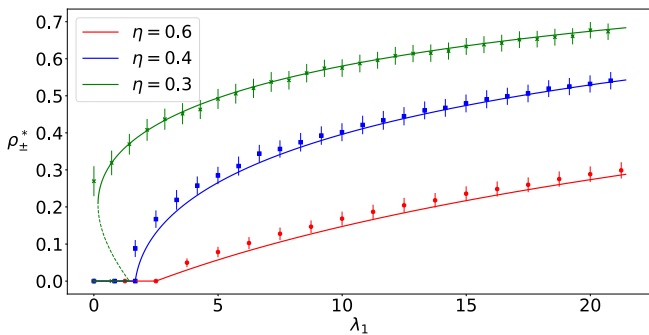


FIG. 4. Prevalence  $\rho_{\pm}^*$  as a function of  $\lambda_1$  for several values of  $\eta$  and  $\mu = 0.07$ ,  $\gamma_1 = 0.3$ ,  $\gamma_2 = 0.2$ ,  $\gamma_3 = 0$ ,  $\gamma_4 = 0.2$ ,  $\gamma_5 = 0$ ,  $\beta_2 = 0.04$ ,  $\langle k \rangle = 60$  and  $\langle k_{\Delta} \rangle = 10$ . Stochastic simulations (symbols) obtained with an implementation of the Gillespie algorithm are shown together with the mean-field prediction (the stable and unstable equilibria predicted by the mean-field model are respectively shown with solid and dashed lines). Each symbol is the average over several independent stochastic realizations, obtained for synthetic simplicial complexes of 500 nodes (see the main text and Appendix B for a description of the algorithm used to generate the synthetic simplicial complexes); the standard deviation is also reported (vertical bars).

The results shown in the figure allow us to appreciate the substantial impact that distrust has on the social contagion. First, we observe that for a given  $\lambda_1$ , which is above the epidemic threshold,  $\rho^*$  decreases as  $\eta$  increases. Hence, the larger is the distrust in the network the lower is the fraction of people that are infected at equilibrium. Even more interestingly, the presence of trust and distrust relationships conditions the nature of the transition from the disease-free state to the endemic one, and so the existence of a bistable regime. In particular, we observe that increasing the amount of distrust in the network makes the bistability region to shrink until it vanishes, with the transition at  $\lambda_1 = 1/(1 - \eta)$  becoming continuous. Mathematically, this means that by tuning the value of  $\eta$  we can shift from a case where  $\Lambda > 1 + \lambda_2$ , i.e., the bistability region exists, to one where  $\Lambda < 1 + \lambda_2$ , i.e., a bistable regime is not allowed.

### B. Non-monotonic behavior of the prevalence

Let us now investigate how the infection depends on the average degree  $\langle k \rangle$ . In Fig. 5, we show the prevalence  $\rho_+^*$  as a function of the distrust  $\eta$  for two particular values of the average node degree  $\langle k \rangle$ . The other parameters are identical to those used in Fig. 4, but  $\beta_1 = 0.003$ . Each curve corresponds thus to a fixed different value of  $\lambda_1$ . Let us consider the blue and red curves corresponding respectively to  $\langle k \rangle = 60$  and  $\langle k \rangle = 120$ . The associated values of  $\lambda_1$  (resp.  $\sim 2.57$  and  $\sim 5.14$ ) are large enough so that the system is never bistable regardless of  $\eta$  (see Fig. 4).

As we have already seen, the lower the fraction of distrust and the larger the infection. We observe that, while the prevalence is monotonic and continuous with respect to  $\eta$ , it is non-monotonic with respect to the average connectivity  $\langle k \rangle$ . Indeed, both prevalence curves cross each other at two distinct values of  $\eta$ , namely at  $0 < \eta_1 < \eta_2 < 1$  with  $\eta_1$  almost zero and  $\eta_2 \approx 0.4$  (see Appendix C). This implies that for  $\eta_1 < \eta < \eta_2$ , increasing the connectivity of the network reduces the prevalence while the opposite phenomenon takes place for large values of the distrust, i.e., for  $\eta > \eta_2$ .

This behavior apparently looks counter-intuitive. For a given value of  $\eta$ , the only parameters changing as a function of  $\langle k \rangle$  are  $\lambda_1$  and  $\lambda_2$ . Therefore, the magnitude of the prevalence with respect to the average degree will depend on the relative strength between these two parameters, which are associated to pairwise infections and recoveries, respectively. Let us observe that a similar phenomenon can be observed if  $\beta_1 = \beta_2$  even if less pronounced (see Fig. 11 in the Appendix C). The inset in Fig. 5 shows the joint dependence of the epidemic prevalence  $\rho_+^*$  on  $\eta$  and  $\langle k \rangle$ . For a given value of  $\langle k \rangle$ , the prevalence decreases as the fraction of distrust increases. At contrast, for a given value of  $\eta$ , the behaviour of the prevalence as a function of  $\langle k \rangle$  depends on the value of  $\eta$ . For small values of  $\eta$ , the prevalence decreases as  $\langle k \rangle$  is increased while the opposite phenomenon takes place for larger values of  $\eta$ .

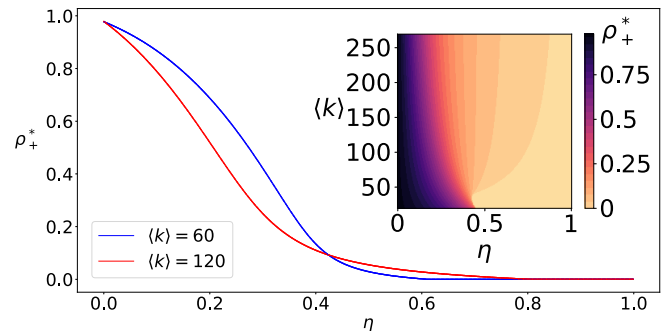


FIG. 5. Prevalence as a function of  $\eta$ , for various values of  $\langle k \rangle$ ,  $\beta_1 = 0.003$  and remaining parameters identical to those of Fig. 4. Inset: Level sets of the infection  $\rho_+^*$  as a function of the parameters  $\langle k \rangle$  and  $\eta$ ,  $\beta_1 = 0.003$  and remaining parameters identical to those of Fig. 4.

## V. THE SOCIAL BALANCE THEORY

The model presented in the previous section is based on the assumption that agents maintain the same pairwise trust/distrust relations when they are involved in interactions in group of more than two mates. This assumption implies that the distribution of signed triangles depends on the fraction of negative links in the network,  $\eta$ , and not on a peculiar combination of “+” and “-” inside

each triad. However social balance theory affirms that in a social network, the fraction of balanced triangles, i.e., triadic relations with an odd number of positive links, is larger than the one we would obtain if signs were randomly distributed [30–32, 42], the rationale being that individuals try to reduce the tensions originating from the presence of an even number of negative relations. In this section we extend the previous model in order to investigate the role of balanced and unbalanced triads on social contagion. This can be achieved by introducing new parameters,  $p_i \geq 0$ , where  $i = 0, \dots, 3$ , refers to the number of positive links in the triads, to express the excess or the deficiency of peculiar signed 2-simplices with respect to the case where these inherit the signs of the links. This allows us to write

$$\begin{aligned} \tau_0 &= p_0 \eta^3 \langle k_\Delta \rangle, \tau_1 = 3p_1 \eta^2 (1 - \eta) \langle k_\Delta \rangle \\ \tau_2 &= 3p_2 \eta (1 - \eta)^2 \langle k_\Delta \rangle \text{ and } \tau_3 = p_3 (1 - \eta)^3 \langle k_\Delta \rangle. \end{aligned} \quad (7)$$

The model presented in the previous section, i.e., where all the signs were randomly attributed to the edges, can be recovered with the choice  $p_i = 1$  for all  $i$ . If there were only balanced triangles, then  $p_0 = p_2 = 0$ , while  $p_1 = p_3 = 0$  denotes the complete absence of balanced triangles. Let us note that the parameters  $p_i$  are not independent from each other as we must have  $\sum_i \tau_i = \langle k_\Delta \rangle$ , hence

$$p_0 \eta^3 + 3p_1 \eta^2 (1 - \eta) + 3p_2 \eta (1 - \eta)^2 + p_3 (1 - \eta)^3 = 1. \quad (8)$$

Let us observe that the solutions of Eq. (1) are still given by  $\rho_0^* = 0$  and  $\rho_\pm^*$  obtained by (3), of course with new parameters  $\Lambda_i$ ,  $i = 1, \dots, 5$  depending on the new definitions of  $\tau_k$ ,  $k = 0, \dots, 3$  given by (7). The same analysis above performed concerning the existence and stability of the stationary densities can be straightforwardly adapted to the present case.

In the following, we examine how the distribution of distrust relations influences the contagion outcome. As a first analysis, we set the bias parameters relative to balanced triangles to be equal, i.e.,  $p_1 = p_3$ , and we investigate the impact on the contagion of the parameters relative to unbalanced triangles, i.e.,  $p_0$  and  $p_2$ . In Fig. 6 we show the prevalence curves for two values of  $p_0$ , i.e.,  $p_0 = 1$  (red curve) and  $p_0 = 5$  (blue curve), while fixing  $p_2 = 1$ , the values of the other parameters are reported in the caption. Notice that the value of  $p_1 = p_3$  is automatically adapted as to satisfy Eq. (8). Note also that  $\eta$  is fixed, meaning that the average number of negative links is constant. In the same Figure we compare the mean-field solution (curves) with the results of stochastic simulations performed using the Gillespie algorithm (points); the agreement is again satisfactory, the discrepancy being due to finite size effects and the sparsity of the network structure that enhance correlations, neglected in the construction of the mean-field model (see Appendix B for more details).

We can observe two opposite behaviors. On the one hand, for small values of  $\lambda_1$ , the prevalence  $\rho^*$  increases

when reducing  $p_0$ , i.e., decreasing the number of unbalanced triangles (the red curve is above the blue one). On the other hand, for large values of  $\lambda_1$ , we find on the contrary that  $\rho^*$  increases as we increase  $p_0$  (the red curve is below the blue one). This implies the existence of a value  $\lambda_{\text{cross}}$  at which both curves have the same prevalence. The prevalence at the particular value  $\lambda_{\text{cross}}$  can be computed explicitly (see Appendix D) and is given, by assuming  $\eta = 1/2$ ,  $p_1 = p_3$  and  $p_2 = 1$  by:

$$\rho^*(\lambda_{\text{cross}}) = \frac{\gamma_1}{\gamma_1 + \gamma_4 - 4\gamma_5}, \quad (9)$$

provided the parameters  $\gamma_4 > 4\gamma_5$  to ensure the prevalence to lie into  $(0, 1)$ . For the parameters used in Fig. 6, we obtain  $\rho^*(\lambda_{\text{cross}}) = 7/17 \sim 0.41$ .

To further investigate the crossing behavior, we construct the phase diagram of  $\rho^*$  as a function of  $p_0$  and  $\lambda_1$ . This is shown in the inset of Fig. 6. For large values of  $\lambda_1$  (right of the dashed green line), the prevalence increases as we increase  $p_0$ , while the opposite holds true for small values of  $\lambda_1$  (left of the dashed green line). Note that the black region corresponds to the parameter set for which the disease-free state is the only stable equilibrium.

These results highlight how the effect of balanced and unbalanced triangles on the prevalence highly depends on the link infectivity of the process. As already stated, real social systems are more likely composed by balanced configurations, i.e., they are associated to low values of  $p_0$  and  $p_2$ . So in our analysis, we expect a contagion spreading on social networks to show a behavior more similar to that of the red curve. Hence, we would expect real social systems to have larger (resp. smaller) prevalence compared to random sign configurations when the infectivity  $\lambda_1$  is small (resp. large). This counter-intuitive behavior is due to the high nonlinearity of the contagion process, as infection and recovery mechanisms are associated to both balanced and unbalanced triangles (see Fig. 2 and 3).

Finally, we find that by tuning the bias parameter  $p_0$  we can change the nature of the transition from the disease-free state to the endemic one. Indeed, we can observe that the system becomes bistable for low enough values of  $p_0$  (the red curve shows bistability, while the blue curve does not).

We now allow  $p_2$  to vary, thus studying the behavior of the system as a function of both  $p_0$  and  $p_2$ . Still, we assume that  $p_1 = p_3$ , with their value determined by Eq. (8). We first consider the case  $p_0 = p_2$ , hence focusing on the effect of tuning balanced and unbalanced triangles. We recall that for a given value of  $p_0$  (equals to  $p_2$ ), the value of  $p_1$  (equals to  $p_3$ ) is deduced from Eq. (8). Therefore, we can study the state of the system as a function of a single parameter, i.e.,  $p_0$ . The upper panel of Fig. 7 shows the prevalence curves for different values of  $p_0$  and  $p_1$ , with the remaining parameters identical to those of Fig. 6. In particular, we consider  $\eta = 0.5$ , for which we have  $p_0 + p_1 = 2$ . We notice that increasing the proportion of balanced triads has a double

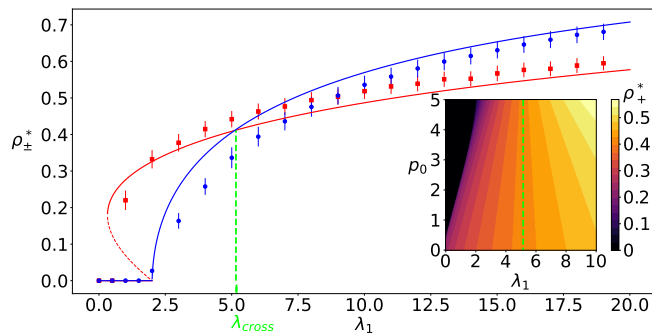


FIG. 6. Prevalence  $\rho_{\pm}^*$  as a function of  $\lambda_1$  for  $p_0 = 1$  (red curve) and  $p_0 = 5$  (blue curve) and fixed parameters  $p_2 = 1$ ,  $\eta = 0.5$ ,  $\langle k \rangle = 60$ ,  $\langle k_{\Delta} \rangle = 10$ ,  $\mu = 0.05$ ,  $\beta_2 = 0.007$ ,  $\gamma_1 = 0.35$ ,  $\gamma_2 = 0.2$ ,  $\gamma_3 = 0$ ,  $\gamma_4 = 0.5$  and  $\gamma_5 = 0$ . The parameters  $p_1 = p_3$  are deduced from Eq. (8) and take the value 1 for  $p_0 = 1$  (red curve) and 0 for  $p_0 = 5$  (blue curve). Points are the average over several independent stochastic simulations performed over synthetic simplicial complexes made of 500 nodes. Inset: Phase diagram of the infection  $\rho_+^*$  as a function of the parameters  $p_0$  and  $\lambda_1$  for the same set of parameters.

effect: on the one hand, it enlarges the bistability region, i.e., higher-order interactions can sustain the spreading for smaller values of  $\lambda_1$ . On the other hand, it tends to reduce the prevalence of the social behavior. We extend this analysis by investigating the contributions of specific unbalanced sign configurations by keeping  $p_1 = p_3$  and varying separately  $p_0$  and  $p_2$ . In the bottom panels of Fig. 7, we show the phase diagram of  $\rho^*$  as function of  $p_0$  and  $p_2$  for  $\lambda_1 = 20$  (left) and  $\lambda_1 = 2$  (right). In both panels, the white region denoted by *A* is such that the values of  $p_0$  and  $p_2$  would imply  $p_1 = p_3 < 0$  which is not physically acceptable. In particular, the delimiting line of region *A* is given by  $p_0\eta^3 + 3p_2\eta(1-\eta)^2 = 1$ , and it corresponds to the case where no balanced triangles are present, i.e.,  $p_1 = p_3 = 0$ . Coherently with the previous analysis, when  $\lambda_1$  is large enough (left panel), the infection increases with  $p_0$  and  $p_2$ . Note that the vertical dashed line represents  $p_2 = 1$ , corresponding to the case previously studied. For  $\lambda_1 = 2$ , the behavior of the system with respect to  $p_0$  and  $p_2$  is more complex. Indeed, for small values of  $p_2$ , the prevalence decreases as  $p_0$  is increases, while the opposite is true for large values of  $p_2$ .

For this latter case, we distinguish two additional zones. In zone *B*, there is no bistability, while the latter is present in zone *C*. The separation line between the two is found for  $\Lambda = 1 + \lambda_2$ , and takes, for the above values of the parameters, the expression,  $p_0 = -\frac{5}{7}p_2 + \frac{984}{175}$ .

To conclude the analysis, we further investigate the impact of the particular configurations of balanced and unbalanced triangles present in the network. In particular, we first fix the values of  $p_1$  and  $p_3$ , namely the bias parameters for the balanced triangles, and vary  $p_0$  and  $p_2$ , so the bias parameters for the unbalanced configurations, then we do the opposite, fixing  $p_0$  and  $p_2$ , and varying  $p_1$  and  $p_3$ .

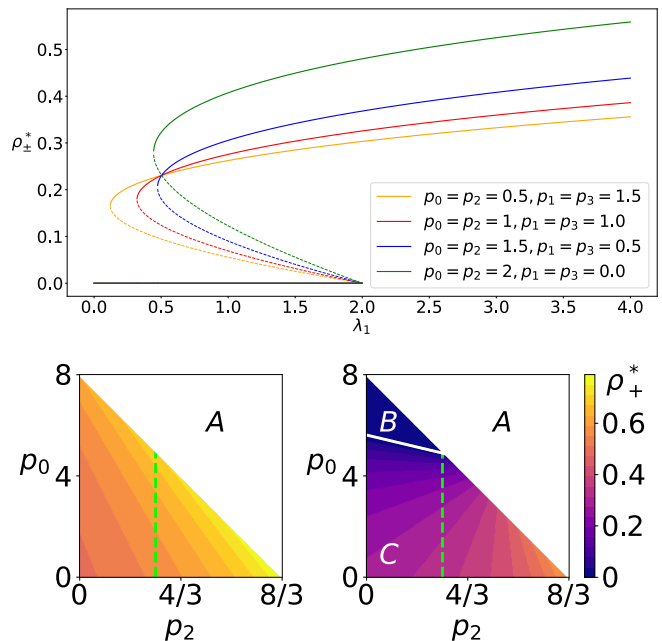


FIG. 7. (Upper panel) Prevalence  $\rho_{\pm}^*$  as a function of  $\lambda_1$  for distinct values of  $p_0 = p_2$  and  $p_1 = p_3$ . The remaining parameters of the model are identical to those of Fig. 6. (Bottom panels) Phase diagram of the infection  $\rho^*$  as a function of the parameters  $p_0$  and  $p_2$  for  $\lambda_1 = 20$  (left) and  $\lambda_1 = 2$  (right) and the remaining parameters identical to those of Fig. 6. The vertical dashed curve (in green) corresponds to  $p_2 = 1$ .

In the top panel of Fig. 8 we report the fraction of infected nodes as a function of  $p_0$  and  $p_2$  for fixed  $p_1 = p_3 = 1$ ; let us remember again that because of the constraint (8)  $p_0$  and  $p_2$  are not independent each other. We can observe that for a fixed  $\lambda_1$ , the larger  $p_2$ , i.e., the more triangles with two positive links, the larger the final infection state. Let us emphasize that  $p_0$ , i.e., the fraction of triangles with no positive links, impacts the system outcome in the opposite direction: the larger the value of the parameter, the smaller the fraction of infected. This comes from the fact that  $p_2$  is associated to the three-body infection process having rates  $\gamma_2$  and  $\gamma_3$  (see Fig. 2), while  $p_0$  is related instead to recoveries occurring at rate  $\gamma_5$  (see Fig. 3). Let us also observe that by increasing  $p_2$ , and thus by decreasing  $p_0$ ,  $\lambda_{\text{crit}}$  decreases and thus the system is more prone to exhibit a bistable regime. Moreover, for a given value of  $\lambda_1$  in the bistability region, we find that the critical amount of infected people needed to converge to the endemic state decreases as  $p_2$  increases. Stated differently, by increasing the number of unbalanced triangles with two positive links, the system can “easily” switch to an endemic state.

In the bottom panel of Fig. 8 we show the results corresponding to a variation of  $p_1$ , and thus  $p_3$ , for fixed  $p_0 = p_2 = 1$ . Again the two parameters have opposite impact: by increasing  $p_3$  (resp.  $p_1$ ), the infection  $\rho^*$  increases (resp. decreases). Similarly to the previous case,

$p_3$  is associated to three-body infections occurring at rate  $\gamma_1$ , while  $p_1$  is linked to recoveries occurring at rate  $\gamma_4$ . Coherently, when we increase the value of  $p_3$  a bistable regime can emerge.

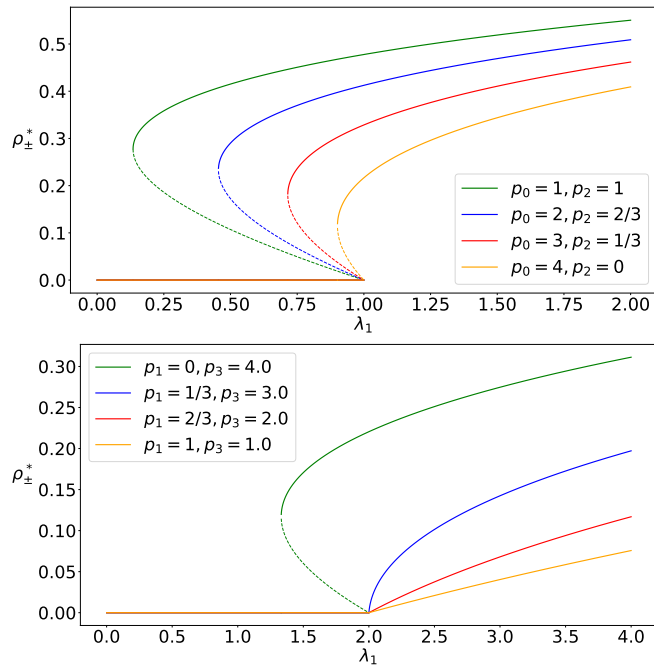


FIG. 8. Top: Fraction  $\rho^*$  of infected nodes as a function of  $\lambda_1$  for distinct values of  $p_0$  and  $p_1 = p_3 = 1$ ,  $\eta = 0.5$ ,  $\mu = 0.05$ ,  $\beta_2 = 0.01$ ,  $\gamma_1 = 0.15$ ,  $\gamma_2 = 0.1$ ,  $\gamma_3 = 0$ ,  $\gamma_4 = 0.05$ ,  $\gamma_5 = 0$ ,  $\langle k \rangle = 30$  and  $\langle k_\Delta \rangle = 15$ . Bottom: Fraction  $\rho^*$  of infected nodes as a function of  $\lambda_1$  for distinct values of  $p_1$  and  $p_0 = p_2 = 1$ ,  $\eta = 0.5$ ,  $\mu = 0.05$ ,  $\beta_2 = 0.06$ ,  $\gamma_1 = 0.15$ ,  $\gamma_2 = 0.05$ ,  $\gamma_3 = 0$ ,  $\gamma_4 = 0.05$ ,  $\gamma_5 = 0$ ,  $\langle k \rangle = 30$  and  $\langle k_\Delta \rangle = 15$ .

Overall these results suggest that the bias parameters  $p_i$  strongly impact the outcome of the contagion process, both in terms of its final prevalence and of its dynamics, i.e., continuous and discontinuous transitions, in a nontrivial way. Also, our model highlights that not only the relative proportion of balanced and unbalanced triangles determines the contagion, but also the particular configurations within these two classes can have a crucial influence on the system.

## VI. CONCLUSION

In this paper we have introduced a model of complex contagion on signed higher-order networks, which has allowed us to investigate, both numerically and analytically, the combined effect of group interactions and distrust relations on the dynamics of social contagion. In the proposed model, a social system with group interactions is represented as a signed simplicial complex, in which the edges are attributed either a “+” or a “-” sign to respectively denote trust or distrust between agents. In our model, we have two states, i.e., nodes can either

be in the infected state (if they have adopted an opinion or a social norm) or the susceptible state (if they can adopt). The existence of signed relations allows for additional infection and recovery channels, which generalize those in the simplicial contagion model [15]. Namely an infected agent can become susceptible because of a signed three-body interaction. Two variants of the model were considered: in the first one, edge signs were attributed randomly and maintained the same during a group interaction, while in the second one the distribution of signs in the triadic groups was biased so as to account for social balance theory. With the first variant of the model, we have highlighted how trust and distrust relations affect the transition of a system from a disease-free state to an endemic one. Specifically, we have shown that increasing distrust can change the nature of the transition from discontinuous to continuous, by making the bistability region associated with the first-order transition vanish. This extends previous results obtained on contagion in the presence of group interactions [15], by pointing out the crucial role played by trust in the spreading process. Moreover, we have characterized the nontrivial interplay existing between the fraction of distrust relations and the connectivity of the social network in shaping the collective dynamics of the system. With the second variant of the model, we have analyzed how the precise patterns of trust/distrust relations impact complex contagion in higher-order networks. In particular, we have highlighted how the contagion is determined not only by the relative proportion of balanced and unbalanced triangles, but also by which configuration within these two classes is more frequent. Various extensions of the present work are possible. First of all, it would be interesting to perform some numerical simulations on real (signed) higher-order networks and compare the results to the ones obtained with synthetic ones. Also, it would be useful to generalize the model by considering larger group structures, e.g., groups of size 4, and the new infection and recovery channels related to those larger groups. The analysis of a contagion model evolving on 3-simplices can be of interest as there are configurations where no clear majority exists (i.e., two individuals spread the diseases while two other do not), thus opening for further microscopic mechanisms. Let us observe that structurally balanced higher-order structures can be defined by using Harary balance theorem, stating that signed a graph is structurally balanced if and only if there is no cycle with an odd number of negative edges [32]. A third research direction would be to allow the pattern of contacts to change over time or the signed relations and nodes states to co-evolve. Finally, it would be interesting to consider an heterogeneous mean-field approach to better investigate the impact of the structural properties of higher-order networks on contagion.

## VII. ACKNOWLEDGMENTS

J.F.D.K. is supported by a FNRS Aspirant Fellowship under the Grant FC38477. Part of the results were obtained using the computational resources provided by the “Consortium des Equipements de Calcul Intensif” (CECI), funded by the Fonds de la Recherche

Scientifique de Belgique (F.R.S.-FNRS) under Grant No. 2.5020.11 and by the Walloon Region. L.G. acknowledges the Erasmus+ program for funding his visit in the group of T.C. V.L. acknowledges support from the European Union, NextGenerationEU, GRINS project (GRINS PE00000018 - CUP E63C22002120006).

- 
- [1] A. Barrat, M. Barthelemy, and A. Vespignani, *Dynamical processes on complex networks*. Cambridge university press, 2008.
- [2] D. Centola and M. Macy, “Complex contagions and the weakness of long ties,” *American journal of Sociology*, vol. 113, no. 3, pp. 702–734, 2007.
- [3] R. Pastor-Satorras, C. Castellano, P. Van Mieghem, and A. Vespignani, “Epidemic processes in complex networks,” *Reviews of modern physics*, vol. 87, no. 3, p. 925, 2015.
- [4] A. L. Hill, D. G. Rand, M. A. Nowak, and N. A. Christakis, “Infectious disease modeling of social contagion in networks,” *PLOS computational biology*, vol. 6, no. 11, p. e1000968, 2010.
- [5] S. Lehmann and Y.-Y. Ahn, “Complex spreading phenomena in social systems,” *Computational Social Sciences*, vol. 10, pp. 978–3, 2018.
- [6] I. Z. Kiss, J. C. Miller, P. L. Simon, *et al.*, “Mathematics of epidemics on networks,” *Cham: Springer*, vol. 598, p. 31, 2017.
- [7] G. Shi, C. Altafini, and J. S. Baras, “Dynamics over signed networks,” *SIAM Review*, vol. 61, no. 2, pp. 229–257, 2019.
- [8] V. Latora, V. Nicosia, and G. Russo, *Complex networks: principles, methods and applications*. Cambridge University Press, 2017.
- [9] G. Ghasemiesfeh, R. Ebrahimi, and J. Gao, “Complex contagion and the weakness of long ties in social networks: revisited,” in *Proceedings of the fourteenth ACM conference on Electronic Commerce*, pp. 507–524, 2013.
- [10] F. D. Malliaros, M.-E. G. Rossi, and M. Vazirgiannis, “Locating influential nodes in complex networks,” *Scientific reports*, vol. 6, no. 1, pp. 1–10, 2016.
- [11] S. Pei and H. A. Makse, “Spreading dynamics in complex networks,” *Journal of Statistical Mechanics: Theory and Experiment*, vol. 2013, no. 12, p. P12002, 2013.
- [12] Z. Ruan, G. Iniguez, M. Karsai, and J. Kertész, “Kinetics of social contagion,” *Physical review letters*, vol. 115, no. 21, p. 218702, 2015.
- [13] E. Lee and P. Holme, “Social contagion with degree-dependent thresholds,” *Physical Review E*, vol. 96, no. 1, p. 012315, 2017.
- [14] W. Wang, M. Tang, P. Shu, and Z. Wang, “Dynamics of social contagions with heterogeneous adoption thresholds: crossover phenomena in phase transition,” *New Journal of Physics*, vol. 18, no. 1, p. 013029, 2016.
- [15] I. Iacopini, G. Petri, A. Barrat, and V. Latora, “Simplicial models of social contagion,” *Nature communications*, vol. 10, no. 1, pp. 1–9, 2019.
- [16] F. Battiston, G. Cencetti, I. Iacopini, V. Latora, M. Lucas, A. Patania, J.-G. Young, and G. Petri, “Networks beyond pairwise interactions: structure and dynamics,” *Physics Reports*, vol. 874, pp. 1–92, 2020.
- [17] F. Battiston, E. Amico, A. Barrat, G. Bianconi, G. Ferraz de Arruda, B. Franceschiello, I. Iacopini, S. Kéfi, V. Latora, Y. Moreno, *et al.*, “The physics of higher-order interactions in complex systems,” *Nature Physics*, vol. 17, no. 10, pp. 1093–1098, 2021.
- [18] S. Majhi, M. Perc, and D. Ghosh, “Dynamics on higher-order networks: A review,” *Journal of the Royal Society Interface*, vol. 19, no. 188, p. 20220043, 2022.
- [19] G. Bianconi, *Higher-order networks*. Cambridge University Press, 2021.
- [20] C. Bick, E. Gross, H. A. Harrington, and M. T. Schaub, “What are higher-order networks?,” *SIAM Review*, vol. 65, no. 3, pp. 686–731, 2023.
- [21] G. F. de Arruda, G. Petri, and Y. Moreno, “Social contagion models on hypergraphs,” *Physical Review Research*, vol. 2, no. 2, p. 023032, 2020.
- [22] N. W. Landry and J. G. Restrepo, “The effect of heterogeneity on hypergraph contagion models,” *Chaos: An Interdisciplinary Journal of Nonlinear Science*, vol. 30, no. 10, p. 103117, 2020.
- [23] S. Chowdhary, A. Kumar, G. Cencetti, I. Iacopini, and F. Battiston, “Simplicial contagion in temporal higher-order networks,” *Journal of Physics: Complexity*, vol. 2, no. 3, p. 035019, 2021.
- [24] A. Barrat, G. Ferraz de Arruda, I. Iacopini, and Y. Moreno, “Social contagion on higher-order structures,” in *Higher-Order Systems*, pp. 329–346, Springer, 2022.
- [25] G. St-Onge, I. Iacopini, V. Latora, A. Barrat, G. Petri, A. Allard, and L. Hébert-Dufresne, “Influential groups for seeding and sustaining nonlinear contagion in heterogeneous hypergraphs,” *Communications Physics*, vol. 5, no. 1, p. 25, 2022.
- [26] G. Ferraz de Arruda, G. Petri, P. M. Rodriguez, and Y. Moreno, “Multistability, intermittency, and hybrid transitions in social contagion models on hypergraphs,” *Nature Communications*, vol. 14, no. 1, p. 1375, 2023.
- [27] M. Saeedian, N. Azimi-Tafreshi, G. Jafari, and J. Kertesz, “Epidemic spreading on evolving signed networks,” *Physical Review E*, vol. 95, no. 2, p. 022314, 2017.
- [28] S. Unicomb, G. Iniguez, and M. Karsai, “Threshold driven contagion on weighted networks,” *Scientific reports*, vol. 8, no. 1, p. 3094, 2018.
- [29] H.-J. Li, W. Xu, S. Song, W.-X. Wang, and M. Perc, “The dynamics of epidemic spreading on signed networks,” *Chaos, Solitons & Fractals*, vol. 151, p. 111294, 2021.
- [30] F. Heider, “Attitudes and cognitive organization,” *The Journal of psychology*, vol. 21, no. 1, pp. 107–112, 1946.
- [31] F. Harary, “On the notion of balance of a signed graph,” *Michigan Mathematical Journal*, vol. 2, no. 2, pp. 143–

- 146, 1953.
- [32] D. Cartwright and F. Harary, “Structural balance: A generalization of heider’s theory,” *Psychological Rev.*, vol. 63, p. 277, 1956.
- [33] J. Leskovec, D. Huttenlocher, and J. Kleinberg, “Signed networks in social media,” in *Proceedings of the SIGCHI conference on human factors in computing systems*, pp. 1361–1370, 2010.
- [34] X. Zheng, D. Zeng, and F.-Y. Wang, “Social balance in signed networks,” *Information Systems Frontiers*, vol. 17, no. 5, pp. 1077–1095, 2015.
- [35] A. Kirkley, G. T. Cantwell, and M. E. Newman, “Balance in signed networks,” *Physical Review E*, vol. 99, no. 1, p. 012320, 2019.
- [36] E. David and J. Kleinberg, *Networks, Crowds, and Markets: Reasoning about a Highly Connected World*. Cambridge University Press, 2010.
- [37] D. T. Gillespie, “Exact stochastic simulation of coupled chemical reactions,” *J Phys Chem*, vol. 81, pp. 2340–2361, 1977.
- [38] J. R. Munkres, *Elements of algebraic topology*. CRC press, 2018.
- [39] G. Cencetti, F. Battiston, B. Lepri, and M. Karsai, “Temporal properties of higher-order interactions in social networks,” *Scientific reports*, vol. 11, no. 1, p. 7028, 2021.
- [40] I. Iacopini, B. Schäfer, E. Arcaute, C. Beck, and V. Latora, “Multilayer modeling of adoption dynamics in energy demand management,” *Chaos: An Interdisciplinary Journal of Nonlinear Science*, vol. 30, no. 1, p. 013153, 2020.
- [41] C. Altafini, “Consensus problems on networks with antagonistic interactions,” *IEEE transactions on automatic control*, vol. 58, no. 4, pp. 935–946, 2012.
- [42] M. Szell, R. Lambiotte, and S. Thurner, “Multirelational organization of large-scale social networks in an online world,” *Proceedings of the National Academy of Sciences*, vol. 107, no. 31, pp. 13636–13641, 2010.
- [43] C. Cianci and T. Carletti, “Stochastic patterns in a 1d rock-paper-scissors model with mutation,” *Physica A: Statistical Mechanics and its Applications*, vol. 410, p. 66, 2014.
- [44] T. Carletti and A. Filisetti, “The stochastic evolution of a protocell: The gillespie algorithm in a dynamically varying volume,” *Computational and Mathematical Methods in Medicine*, vol. 2012, p. 13, 2012.
- [45] J. P. Gleeson, S. Melnik, J. A. Ward, M. A. Porter, and P. J. Mucha, “Accuracy of mean-field theory for dynamics on real-world networks,” *Physical Review E*, vol. 85, no. 2, p. 026106, 2012.
- [46] W. Wang, M. Tang, H. E. Stanley, and L. A. Braunstein, “Unification of theoretical approaches for epidemic spreading on complex networks,” *Reports on progress in physics*, vol. 80, no. 3, p. 036603, 2017.
- [47] F. Malizia, L. Gallo, M. Frasca, V. Latora, and G. Russo, “Individual-and pair-based models of epidemic spreading: Master equations and analysis of their forecasting capabilities,” *Physical Review Research*, vol. 4, no. 2, p. 023145, 2022.
- [48] F. Malizia, L. Gallo, M. Frasca, V. Latora, and G. Russo, “A pair-based approximation for simplicial contagion,” *arXiv preprint arXiv:2307.10151*, 2023.
- [49] J. T. Matamalas, S. Gómez, and A. Arenas, “Abrupt phase transition of epidemic spreading in simplicial complexes,” *Physical Review Research*, vol. 2, no. 1, p. 012049, 2020.
- [50] G. Burgio, S. Gómez, and A. Arenas, “Triadic approximation for contagions on higher-order networks,” *arXiv preprint arXiv:2306.11441*, 2023.

### Appendix A: Stability analysis of the fixed points

Let us recall that the time evolution of the fraction  $\rho(t)$  of infected nodes in the mean-field limit is ruled out by:

$$\frac{d\rho}{dt} = \rho (a + b\rho + c\rho^2) ,$$

where

$$\begin{aligned} a &= -\mu + \beta_1(1 - \eta)\langle k \rangle \\ b &= -\beta_1(1 - \eta)\langle k \rangle - \beta_2\eta\langle k \rangle + \gamma_1\tau_3 + \frac{\gamma_2\tau_2}{3} + \frac{2\gamma_3\tau_2}{3} \\ c &= -\gamma_1\tau_3 - \frac{\gamma_2\tau_2}{3} - \frac{2\gamma_3\tau_2}{3} - \frac{\gamma_4}{3}\tau_1 - \gamma_5\tau_0 . \end{aligned}$$

One can recast the above temporal evolution as

$$\frac{d\rho}{dt} = -\mu\rho \left( \rho^2(\Lambda + \tilde{\Lambda}) + \rho(\tilde{\lambda}_1 + \lambda_2 - \Lambda) + 1 - \tilde{\lambda}_1 \right) , \quad (\text{A1})$$

where  $\Lambda := \Lambda_1 + \Lambda_2 + \Lambda_3$  and  $\tilde{\Lambda} := \Lambda_4 + \Lambda_5$  with:

$$\begin{aligned}\Lambda_1 &= \frac{\gamma_1 \tau_3}{\mu}, \Lambda_2 = \frac{\gamma_2 \tau_2}{3\mu}, \Lambda_3 = \frac{2\gamma_3 \tau_2}{3\mu}, \\ \Lambda_4 &= \frac{\gamma_4 \tau_1}{3\mu} \text{ and } \Lambda_5 = \frac{\gamma_5 \tau_0}{\mu}, \\ \tilde{\lambda}_1 &:= \lambda_1(1 - \eta) = \frac{\beta_1 \langle k \rangle}{\mu}(1 - \eta), \lambda_2 = \frac{\beta_2 \eta \langle k \rangle}{\mu}.\end{aligned}$$

It follows that the system admits three fixed points, namely  $\rho_0^* = 0$  and  $\rho_{\pm}^*$  with

$$\rho_{\pm}^* = \frac{\Lambda - \tilde{\lambda}_1 - \lambda_2 \pm \sqrt{(\Lambda - \tilde{\lambda}_1 - \lambda_2)^2 - 4(\Lambda + \tilde{\Lambda})(1 - \tilde{\lambda}_1)}}{2(\Lambda + \tilde{\Lambda})}. \quad (\text{A2})$$

The fixed points  $\rho_{\pm}^*$  are physically acceptable provided they are positive and belong to the interval  $[0, 1]$ . Let us first investigate the conditions on  $\tilde{\lambda}_1$  for the roots  $\rho_{\pm}^*$  to be real. This is done by investigating the sign of the radicand. We have:

$$(\Lambda - \tilde{\lambda}_1 - \lambda_2)^2 - 4(\Lambda + \tilde{\Lambda})(1 - \tilde{\lambda}_1) = 0 \iff \tilde{\lambda}_1 = -(\lambda_2 + \Lambda + 2\tilde{\Lambda}) \pm 2\sqrt{(\Lambda + \tilde{\Lambda})(1 + \lambda_2 + \tilde{\Lambda})}.$$

Denoting by  $\lambda_{\text{crit}} := -(\lambda_2 + \Lambda + 2\tilde{\Lambda}) + 2\sqrt{(\Lambda + \tilde{\Lambda})(1 + \lambda_2 + \tilde{\Lambda})}$ , this means that if  $0 \leq \tilde{\lambda}_1 < \lambda_{\text{crit}}$ , the radicand is negative and thus  $\rho_0^* = 0$  is the only physical solution, obviously stable, as follows directly upon rewriting Eq. (A1) as:

$$\frac{d\rho}{dt} = -\mu\rho(\rho - \rho_+^*)(\rho - \rho_-^*). \quad (\text{A3})$$

If  $\tilde{\lambda}_1 > \lambda_{\text{crit}}$ , then  $\rho_-^*$  and  $\rho_+^*$  are both real. One can also show that  $\rho_+^* < 1$ . Indeed, one has:

$$\begin{aligned}\rho_+^* < 1 &\iff \frac{\Lambda - \tilde{\lambda}_1 - \lambda_2 + \sqrt{(\Lambda - \tilde{\lambda}_1 - \lambda_2)^2 - 4(\Lambda + \tilde{\Lambda})(1 - \tilde{\lambda}_1)}}{2(\Lambda + \tilde{\Lambda})} < 1 \\ &\iff \sqrt{(\Lambda - \tilde{\lambda}_1 - \lambda_2)^2 - 4(\Lambda + \tilde{\Lambda})(1 - \tilde{\lambda}_1)} < \Lambda + 2\tilde{\Lambda} + \tilde{\lambda}_1 + \lambda_2 \\ &\iff \tilde{\Lambda} + 1 + \lambda_2 > 0,\end{aligned}$$

where the last line was obtained upon straightforward computations. This last condition is always satisfied since  $\tilde{\Lambda}$  and  $\lambda_2$  are both positive. If  $\tilde{\lambda}_1 > 1$ , then  $\rho_-^*$  is negative (see Eq. (A2)) while  $\rho_+^*$  is positive and, by virtue of the previous computations, below 1. It follows that  $\rho_+^*$  is the only physical stable solution. It remains to investigate the case where  $\lambda_{\text{crit}} < \tilde{\lambda}_1 < 1$ . We distinguish between two cases:

- If  $\Lambda - 1 - \lambda_2 < 0$ , then  $\rho_0^*$  is the only acceptable solution since  $\rho_+^*$  and  $\rho_-^*$  are both negative. It is stable, as can be seen from Eq. (A3). Therefore, in this condition the system will always converge to a disease-free state.
- If  $\Lambda - 1 - \lambda_2 > 0$ , then  $\rho_-^*$  and  $\rho_+^*$  are both physically acceptable, i.e., they are both positive and less than 1. Using Eq. (A3), we deduce that  $\rho_-^*$  is unstable while  $\rho_+^*$  is stable. Also, the disease-free equilibrium  $\rho_0^*$  is stable. Therefore, in this configuration the system is bistable.

## Appendix B: Stochastic simulations

In this appendix, we explain the procedure employed to generate (synthetic) signed simplicial complexes. We also briefly recall the implementation of the Gillespie algorithm used to simulate the contagion process on top of simplicial complexes.

To construct a simplicial complex made of  $N$  nodes with an average number  $\langle k \rangle$  of links incident to a node and an average number  $\langle k_{\Delta} \rangle$  of triangles incident to a node, we used the procedure described in [15]. Given a set of  $N$  nodes, we first consider every pair of nodes and connect them with a probability

$$p_1 = \frac{\langle k \rangle - 2\langle k_{\Delta} \rangle}{(N - 1) - 2\langle k_{\Delta} \rangle}.$$

We then run over all the triplets of nodes and promote each of them to a 2-simplex with probability

$$p_2 = \frac{2\langle k_\Delta \rangle}{(N-1)(N-2)}.$$

One can check that such probabilities lead to the desired average degree  $\langle k \rangle$  and hyperdegree  $\langle k_\Delta \rangle$ . Once the simplicial complex is constructed we have to associate signs to links and triangles. In the first model, we consider successively all the links and attribute them a negative sign with a probability  $\eta$  and a positive sign otherwise. Then because we assume the agents keep the same dyadic trust/distrust relations once in the three-body interaction, we check all the 2-simplices and we add the same signs of the three pairwise couples.

In the second model, we take into account social balance theory by using a biased distribution of signs at the level of the triangles. In particular, the pairwise interactions receive a sign with the same process as above, i.e., a “-” sign with a probability  $\eta$  and a “+” sign otherwise. On the other hand the signs of each triangle are assigned with the probabilities given by Eq. (7) for a given choice of  $p_i$ ,  $i = 0, \dots, 3$ , namely we attribute  $i$  positive signs and thus  $3 - i$  negative signs with a probability  $\frac{\tau_i}{\langle k_\Delta \rangle}$ .

As already described in the main text, we performed the stochastic numerical simulations by using the Gillespie algorithm, that we here briefly describe; we refer the interested reader to [37, 43, 44] for more details and other applications of the method. At time  $t_0 = 0$ , we start with a chosen fraction of infected nodes uniformly randomly distributed in the simplicial complex. We then establish a list of all the possible reactions, i.e., interaction channels as given in Figs. 1, 2 and 3, that can occur given the states of the nodes and the structure of the signed simplicial complex. The Gillespie method is able to determine the most probable reaction to occur and the most probable time at which it will take place. By denoting with  $s_i$  the rate associated with the  $i$ -th reaction and by  $a_0 = \sum_{i=1}^M s_i$  the sum of all the rates, we generate two random numbers  $r_1$  and  $r_2$  from the uniform distribution in  $(0, 1)$ . The next reaction that will occur is the  $\mu$ -th with  $\mu$  such that:

$$\sum_{j=1}^{\mu-1} s_j < r_2 a_0 \leq \sum_{j=1}^{\mu} s_j.$$

This reaction will occur at time  $t_1 = t_0 + \tau = \tau$  with

$$\tau = \frac{1}{a_0} \ln(1/r_1).$$

Note that the underlying assumption is that only one node changes its state during each reaction. After updating the state of this node, we recompute the rates  $s_i$ , some of which could have change values depending on the system state and repeat the process until the fraction of infected nodes stabilizes, i.e., fluctuates around the true equilibrium; the latter is expected to be close to the predicted mean-field equilibrium for large and dense enough simplicial complexes.

Fig. 9 compares, for two distinct values of  $\langle k \rangle$  but fixed remaining parameters, the stochastic simulations (points) with respect to the mean-field prediction (continuous curve). The fraction of infected nodes obtained with the Gillespie algorithm was averaged over the last 10% of the orbit (when the system is close to the stationary state). To detect possible bistability, for each value of  $\lambda_1$ , we ran several independent stochastic simulations, with a distinct fraction of initially infected nodes, ranging in  $(0, 1)$ , uniformly randomly distributed among the nodes of the simplicial complex. Each stochastic simulation corresponds to a newly generated simplicial complex satisfying the above constraints on  $\langle k \rangle$ ,  $\langle k_\Delta \rangle$  and the fraction of signed triangles.

Let us observe that for  $\langle k \rangle = 30$ , the stochastic simulations deviate from the mean-field predictions. Nevertheless, increasing the network density, e.g., by taking  $\langle k \rangle = 60$  reduces this discrepancy as can be seen in the right panel for the same value of  $\eta$ . Although mean-field approaches neglect dynamical and structural correlations, there were shown to provide good approximations for a broad range of dynamical processes and network structures [15, 45]. More sophisticated methods have been developed to take into account the dynamical and structural correlations and obtain more accurate approximations of contagion processes in networks [46, 47], simplicial complexes [48, 49], and hypergraphs [50]. Let us conclude this Appendix with a comment regarding the epidemic fade-out. Due to the stochasticity and the finite-size of the system, it may happen that the infection dies out for values of  $\lambda_1$  well above the epidemic threshold. This epidemic fade-out especially occurs when the fraction of infected nodes at time  $t = 0$  is very small. We decided to discard such rare occurrences.

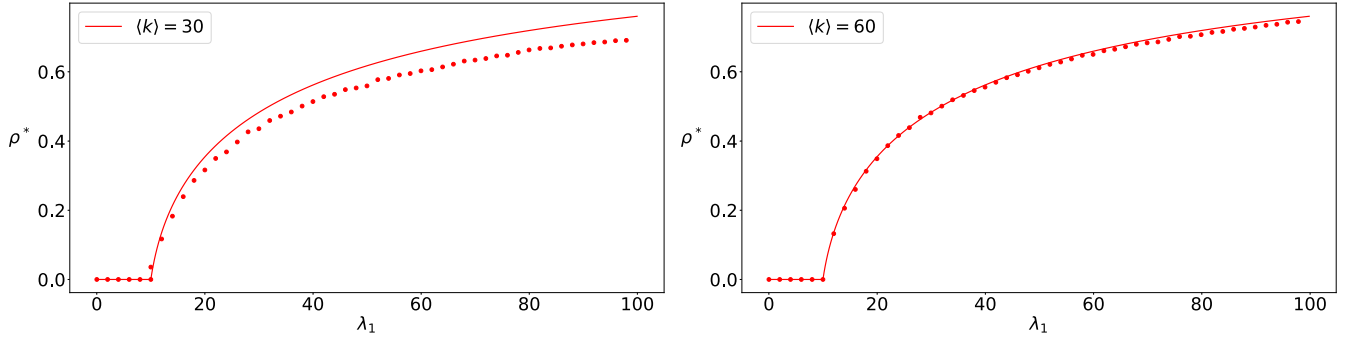


FIG. 9. Prevalence  $\rho^*$  as a function of  $\lambda_1$  in a simplex made by nodes  $N = 1000$  and parameters  $\mu = 0.05$ ,  $\beta_2 = 0$ ,  $\gamma_1 = 0.2$ ,  $\gamma_2 = 0$ ,  $\gamma_3 = 0$ ,  $\gamma_4 = 0.1$ ,  $\gamma_5 = 0$ ,  $\langle k_\Delta \rangle = 15$ ,  $p_0 = 1$ ,  $p_1 = 1$ ,  $p_2 = 1$ ,  $p_3 = 1$ ,  $\eta = 0.9$  with  $\langle k \rangle = 30$  (left panel) and  $\langle k \rangle = 60$  (right panel). The mean-field prediction (continuous curve) is compared with the stochastic simulations (red points) performed by using the Gillespie algorithm.

### Appendix C: Non-monotonicity of the prevalence with respect to the average node degree

In this appendix, we analyze the non-monotonic behavior of the infection as a function of the average node degree  $\langle k \rangle$  and the fraction of distrust  $\eta$  in the network. Let us recall that the stationary density is given by

$$\rho_\pm^* = \frac{\Lambda - \tilde{\lambda}_1 - \lambda_2 \pm \sqrt{(\Lambda - \tilde{\lambda}_1 - \lambda_2)^2 - 4(\Lambda + \tilde{\Lambda})(1 - \tilde{\lambda}_1)}}{2(\Lambda + \tilde{\Lambda})}, \quad (\text{C1})$$

see Eq. (3) in the main text. To highlight the non-monotonic behavior of the infection with respect to the average node degree  $\langle k \rangle$ , we compute the derivative of  $\rho_+^*$  with respect to  $\langle k \rangle$  and determine for which value of  $\eta$  it vanishes. One finds:

$$\frac{d\rho_+^*}{d\langle k \rangle} = \frac{(-\beta_1(1-\eta) - \beta_2\eta) \left[ \sqrt{(\Lambda - \tilde{\lambda}_1 - \lambda_2)^2 - 4(\Lambda + \tilde{\Lambda})(1 - \tilde{\lambda}_1)} + (\Lambda - \tilde{\lambda}_1 - \lambda_2) \right] + 2(\Lambda + \tilde{\Lambda})\beta_1(1-\eta)}{2\mu(\Lambda + \tilde{\Lambda})\sqrt{(\Lambda - \tilde{\lambda}_1 - \lambda_2)^2 - 4(\Lambda + \tilde{\Lambda})(1 - \tilde{\lambda}_1)}}. \quad (\text{C2})$$

From the latter expression, one deduces:

$$\begin{aligned} \frac{d\rho_+^*}{d\langle k \rangle} = 0 &\iff \tilde{\lambda}_1 \left[ \beta_2^2 \eta^2 + \beta_1 \beta_2 \eta (1 - \eta) \right] - \lambda_2 \left[ \beta_1^2 (1 - \eta)^2 + \beta_1 \beta_2 \eta (1 - \eta) \right] - \left[ \beta_1 (1 - \eta) + \beta_2 \eta \right]^2 \\ &\quad - \tilde{\Lambda} \beta_1^2 (1 - \eta)^2 + \Lambda \beta_1 \beta_2 \eta (1 - \eta) = 0 \end{aligned} \quad (\text{C3})$$

Recalling that  $\tilde{\lambda}_1 = \beta_1(1-\eta)\frac{\langle k \rangle}{\mu}$  and  $\lambda_2 = \beta_2\eta\frac{\langle k \rangle}{\mu}$ , we see that the first two terms of the r.h.s of Eq. (C3) cancel each other and we are left with:

$$\frac{d\rho_+^*}{d\langle k \rangle} = 0 \iff g(\eta) := -\left[ \beta_1(1-\eta) + \beta_2\eta \right]^2 - \tilde{\Lambda}(\eta)\beta_1^2(1-\eta)^2 + \Lambda(\eta)\beta_1\beta_2\eta(1-\eta) = 0, \quad (\text{C4})$$

where we have stressed the dependence of  $\Lambda$  and  $\tilde{\Lambda}$  on  $\eta$ . Notice that the latter expression is independent of  $\langle k \rangle$ . Being  $g(\eta)$  a polynomial of degree 5 in  $\eta$ , it has up to 5 real roots in the interval  $(0, 1)$ . As an illustration, let us consider the parameters used in Fig. 5 in the main document. For these parameters, the function  $g$  has two real roots  $\eta_1 < \eta_2$  in the interval  $(0, 1)$  with  $\eta_1$  almost zero and  $\eta_2 \approx 0.4$  as can be seen in the right panel of Fig. 10. Further analysis shows that for  $\eta_1 < \eta < \eta_2$ , the infection decreases as  $\langle k \rangle$  increases (see left panel the curve corresponding to  $\eta = 0.3$ ) while for  $\eta > \eta_2$ , the opposite behavior holds true (see left panel the curve corresponding to  $\eta = 0.5$ ), i.e.,  $\rho^*$  is an increasing function of the average connectivity.

Let us observe that the above effect manifests itself for other choices of parameters, in particular one can assume  $\beta_1 = \beta_2$  and still obtain this phenomenon even if with smaller intensity (see Fig. 11).

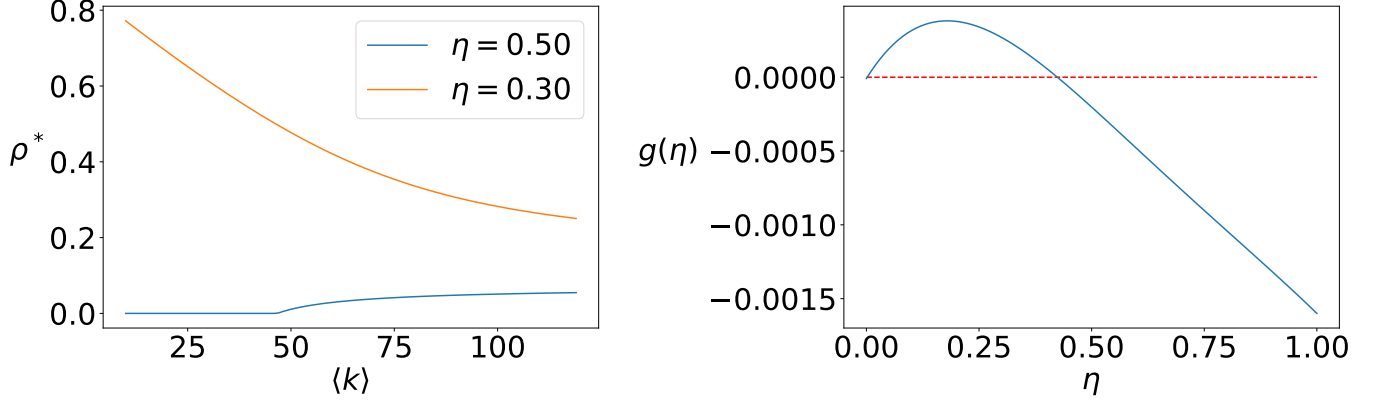


FIG. 10. Left: Infection as a function of the average node degree  $\langle k \rangle$ . When  $\eta_1 < \eta < \eta_2$  with  $g(\eta_1) = 0 = g(\eta_2)$ , the infection decreases with  $\langle k \rangle$  while it is the opposite when  $\eta > \eta_2$   $\eta > \eta_{\text{cross}}$ . The parameters are:  $\beta_1 = 0.003, \beta_2 = 0.04, \gamma_1 = 0.3, \gamma_2 = 0.2, \gamma_3 = 0, \gamma_4 = 0.2, \gamma_5 = 0, \mu = 0.07$  and  $\langle k_\Delta \rangle = 10$ . Right: Plot of the function  $g(\eta)$  for the aforementioned parameters.

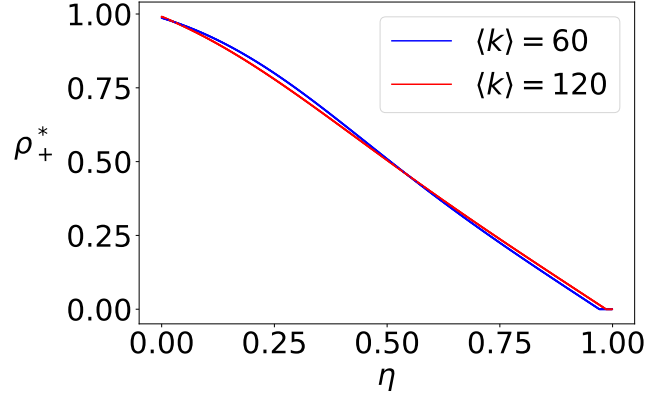


FIG. 11. Prevalence as a function of  $\eta$ , for two distinct values of the average node degree  $\langle k \rangle$  and parameters  $\mu = 0.07, \gamma_1 = 0.3, \gamma_2 = 0.2, \gamma_3 = 0, \gamma_4 = 0.2, \gamma_5 = 0, \beta_1 = \beta_2 = 0.04$  and  $\langle k_\Delta \rangle = 10$ .

#### Appendix D: Conditions for the presence of the crossing phenomenon

The aim of this section is to investigate in more details the crossing behavior observed in Fig. 6 in the main document. Let us start by recalling that stationary densities are solutions of

$$\rho (a + b\rho + c\rho^2) = 0, \quad (\text{D1})$$

where

$$a = -\mu + \beta_1(1 - \eta)\langle k \rangle \quad (\text{D2})$$

$$b = -\beta_1(1 - \eta)\langle k \rangle - \beta_2\eta\langle k \rangle + \gamma_1\tau_3 + \frac{\gamma_2\tau_2}{3} + \frac{2\gamma_3\tau_2}{3} \quad (\text{D3})$$

$$c = -\gamma_1\tau_3 - \frac{\gamma_2\tau_2}{3} - \frac{2\gamma_3\tau_2}{3} - \frac{\gamma_4}{3}\tau_1 - \gamma_5\tau_0. \quad (\text{D4})$$

Let us observe that  $c < 0$  for all values of the parameters, while  $a$  and  $b$  can change signs.

Let us recall the definitions  $\Lambda := \Lambda_1 + \Lambda_2 + \Lambda_3$  and  $\tilde{\Lambda} := \Lambda_4 + \Lambda_5$  with:

$$\Lambda_1 = \frac{\gamma_1\tau_3}{\mu}, \Lambda_2 = \frac{\gamma_2\tau_2}{3\mu}, \Lambda_3 = \frac{2\gamma_3\tau_2}{3\mu}, \Lambda_4 = \frac{\gamma_4\tau_1}{3\mu}, \Lambda_5 = \frac{\gamma_5\tau_0}{\mu}, \lambda_1 = \frac{\beta_1\langle k \rangle}{\mu}, \lambda_2 = \frac{\beta_2\eta\langle k \rangle}{\mu}. \quad (\text{D5})$$

and assume the number of triangles with a given number of positive/negative signs are given by

$$\tau_0 = p_0\eta^3\langle k_\Delta \rangle, \tau_1 = 3p_1\eta^2(1 - \eta)\langle k_\Delta \rangle, \tau_2 = 3p_2\eta(1 - \eta)^2\langle k_\Delta \rangle, \tau_3 = p_3(1 - \eta)^3\langle k_\Delta \rangle. \quad (\text{D6})$$

By dividing (D1) by  $\mu$ , we get  $a/\mu = -1 + \lambda_1(1 - \eta)$  and thus rewrite the non zero solutions  $\rho_{\pm}^*$  as follows

$$\lambda_1(1 - \eta)(1 - \rho_{\pm}^*) = (\rho_{\pm}^*)^2(\Lambda + \tilde{\Lambda}) + \rho_{\pm}^*(\lambda_2 - \Lambda) + 1, \quad (\text{D7})$$

Let us notice that  $\rho_{\pm}^* = 1$  would imply  $\tilde{\Lambda} + \lambda_2 + 1 = 0$  which can never happen being  $\tilde{\Lambda}$  and  $\lambda_2$  positive numbers. Hence, we can write (assuming  $\eta \neq 1$ ):

$$\lambda_1(\rho_{\pm}^*) = \frac{(\rho_{\pm}^*)^2(\Lambda + \tilde{\Lambda}) + \rho_{\pm}^*(\lambda_2 - \Lambda) + 1}{(1 - \rho_{\pm}^*)(1 - \eta)} \quad (\text{D8})$$

Let us observe that  $\lambda_1$  has a vertical asymptote for  $\rho_{\pm}^* = 1$ ; being this function invertible close to  $\rho_{\pm}^* = 1$ , we can conclude that  $\rho_{\pm}^* \rightarrow 1$  for  $\lambda_1 \rightarrow \infty$ .

To have the crossing property, we need to find  $0 < p_0^{(1)} \neq p_0^{(2)}$  such that  $\lambda_1(\rho_{\pm}^*)|_{p_0^{(1)}} = \lambda_1(\rho_{\pm}^*)|_{p_0^{(2)}}$  for some  $0 < \rho^* < 1$  (see Fig. 6); a straightforward computation allows to show that this is equivalent to require:

$$\rho_{\pm}^* = \frac{\phi_1 - \phi_2}{c_2 - c_1}, \quad (\text{D9})$$

here  $\phi_1 := \lambda_2 - \Lambda|_{p_0^{(1)}}$  and  $c_1 := \Lambda + \tilde{\Lambda}|_{p_0^{(1)}}$  and similarly for  $\phi_2$  and  $c_2$ . Let us now consider the case of  $\eta = \frac{1}{2}$  as in Fig. 6 and let us assume  $p_2 = 1$  and  $p_1 = p_3$ . Recalling that  $\tau_0 + \tau_1 + \tau_2 + \tau_3 = \langle k_{\Delta} \rangle$ , we deduce that:

$$p_0 = 5 - 4p_3. \quad (\text{D10})$$

Taking into account the latter condition, one can show upon simplification that:

$$\rho_{\pm}^* = \frac{\gamma_1}{\gamma_1 + \gamma_4 - 4\gamma_5}. \quad (\text{D11})$$

Notice that the latter expression is independent of  $p_3$  and belongs to  $(0, 1)$  provided  $\gamma_4 > 4\gamma_5$ , let us observe that this condition is always met when  $\gamma_5 = 0$  and  $\gamma_4 > 0$ , as considered in our analysis. The corresponding value  $\lambda_{\text{cross}}$  can be deduced from Eq. (D8).